



TITLE:

Morphogenesis of the Inner Ear at Different Stages of Normal Human Development

AUTHOR(S):

Toyoda, Saki; Shiraki, Naoto; Yamada, Shigehito;
Uwabe, Chigako; Imai, Hirohiko; Matsuda, Tetsuya;
Yoneyama, Akio; Takeda, Tohoru; Takakuwa,
Tetsuya

CITATION:

Toyoda, Saki ...[et al]. Morphogenesis of the Inner Ear at Different Stages of Normal Human Development. The Anatomical Record 2015, 298(12): 2081-2090

ISSUE DATE:

2015-12

URL:

<http://hdl.handle.net/2433/216673>

RIGHT:

This is the accepted version of the following article: [Toyoda, S., Shiraki, N., Yamada, S., Uwabe, C., Imai, H., Matsuda, T., Yoneyama, A., Takeda, T. and Takakuwa, T. (2015), Morphogenesis of the Inner Ear at Different Stages of Normal Human Development. Anat Rec, 298: 2081–2090. doi: 10.1002/ar.23268], which has been published in final form at <http://dx.doi.org/10.1002/ar.23268>. This article may be used for non-commercial purposes in accordance with Wiley Terms and Conditions for Self-Archiving; The full-text file will be made open to the public on 17 November 2016 in accordance with publisher's 'Terms and Conditions for Self-Archiving'; This is not the published version. Please cite only the published version.; この論文は出版社版ではありません。引用の際には出版社版をご確認ください。

Morphogenesis of the inner ear at different stages of normal human development

Saki Toyoda¹, Naoto Shiraki¹, Shigehito Yamada^{1,2}, Chigako Uwabe², Hirohiko Imai³,
Tetsuya Matsuda³, Akio Yoneyama⁴, Tohoru Takeda⁴, Tetsuya Takakuwa¹

¹Human Health Science, ²Congenital Anomaly Research Center, Graduate School of Medicine, Kyoto University, Kyoto 606-8507, Japan

³Department of Systems Science, Graduate School of Informatics, Kyoto University, Kyoto 606-8507, Japan

⁴Allied Health Science, Kitazato University, Kanagawa 252-0373, Japan

Running title: 3D morphogenesis of the inner ear

Corresponding author: Dr. Tetsuya Takakuwa

Human Health Science, Graduate School of Medicine, Kyoto University

Sakyo-ku Shogoin Kawahara-cho 53, Kyoto 606-8507, Japan

E-mail: tez@hs.med.kyoto-u.ac.jp

Tel/Fax: +81-75-751-3931

Grant sponsors:

Japan Society for the Promotion of Science and BIRD of the Japan Science and Technology Agency (grant numbers: 22591199, 24119002, 26220004, and 25461642).

Abstract

The present study examined the external morphology and morphometry of the human embryonic inner ear membranous labyrinth and documented its three-dimensional position in the developing embryo using phase-contrast X-ray computed tomography and magnetic resonance imaging. A total of 27 samples between Carnegie stage (CS) 17 and the postembryonic phase during trimester 1 (approximately 6–10 weeks after fertilization) were included. The otic vesicle elongated along the dorso-ventral axis and differentiated into the end lymphatic appendage and cochlear duct (CD) at Carnegie stage (CS) 17. The spiral course of the CD began at CS18, with anterior and posterior semicircular ducts (SDs) forming prominent circles with a common crus. The spiral course of the CD comprised more than two turns at the postembryonic phase, at which time the height of the CD was evident. A linear increase was observed in the length of anterior, posterior, and lateral SDs, in that order, and the length of the CD increased exponentially over the course of development. Bending in the medial direction was observed between the cochlear and vestibular parts from the latero-caudal view, with the angle decreasing during development. The position of the inner ear was stable throughout the period of observation on the lateral to ventral side of the rhombencephalon, caudal to the pontine flexure, and adjacent to the auditory ganglia. The plane of the lateral semicircular canal was approximately 8.0° – 14.6° with respect to the cranial caudal (z-)axis, indicating that the orientation of the inner ear changes during growth to adulthood.

Key words: inner ear, membranous labyrinth, three-dimensional kinetics, human embryo, MR imaging, phase-contrast X-ray CT.

Introduction

The inner ear has an elaborate structure and its development proceeds in a complex manner that can only be fully appreciated by a three-dimensional (3D) analysis. The membranous labyrinth of the inner ear has been subjected to 3D analysis since the introduction of wax plate reconstruction methods (Streeter, 1906), which have been used to model development from embryonic stages to the early fetus (30 mm crown-rump length) (Streeter, 1906; 1917; 1918). However, a staging system was not established at that time and as such, the findings are difficult to reconcile with events ascribed to currently employed Carnegie stages (CS), which are delineated according to the development of external and internal structures and not by size or number of days of development (O’Rahilly and Müller, 1987; 2006).

Subsequent 3D reconstructions have used the CS system, including an investigation of membranous labyrinth development from CS14 to a fetus at 10 weeks of gestation (Arnold and Lang, 2001). We have previously reported a 3D analysis of inner ear development from CS16 to 22 (Yasuda et al., 2007). However, these studies provided limited information, since histological sections used for the reconstruction were prone to deformation and, consequently, inaccuracy. Furthermore, an adequate sample size is required for quantitative evaluations. Thus, a precise morphological and morphometric characterization of inner ear development is still lacking.

Otic capsule formation is initiated parallel to the differentiation of the otic vesicle into the membranous labyrinth starting from CS16 (Arnold and Lang, 2001). The otic capsule becomes the bone labyrinth during fetal development and is lodged between the membranous labyrinth containing endolymph and a corresponding cavity containing perilymph. The membranous and bone labyrinths have similar—though not identical—structures (Hashimoto et al., 2005). The latter has been evaluated from a phylogenetic standpoint given its high degree of conservation between species (Sporer and Zonneveld, 1995; Gunz et al., 2012). The development of the bony labyrinth in the human fetus (9–29 weeks gestation) was recently investigated using high-resolution magnetic resonance imaging (MRI) (Jeffery and Spoor, 2004); the structure attains adult size between 17 and 19 weeks of gestation and is fully encapsulated by bone a few weeks later (Bast et al., 1947). Each part of the bony labyrinth follows distinct developmental kinetics, with some reaching maximum size only after birth (Richard et al., 2010).

The present study investigated the external morphology and morphometry of the human embryonic inner ear membranous labyrinth and its 3D position within the body using phase-contrast X-ray computed tomography (PCXT) and MRI. The results reveal the precise morphological and morphometric growth programs of the inner ear and its limited movement within the body at each CS during the embryonic period.

Materials and Methods

Human embryo specimens

This study was approved by The Committee of Medical Ethics of Kyoto University Graduate School of Medicine, Kyoto, Japan (E986). Approximately 44,000 human embryos comprising the Kyoto Collection are stored at the Congenital Anomaly Research Center of Kyoto University (Nishimura et al., 1968; Shiota, 1991; Yamada et al., 2004). In most cases, pregnancy was terminated during the first trimester for socioeconomic reasons under the Maternity Protection Law of Japan. Some of the specimens (~20%) were undamaged, well-preserved embryos. Aborted embryos brought to the laboratory were measured, examined, and staged using the criteria of O’Rahilly and Müller (1987). A total of 54 inner ear organs from 27 human embryos were selected (CS17, $n = 5$; CS19, $n = 4$; CS18, 20, 21, 22, 23, and postembryonic phase (PE) in trimester 1, $n = 3$ each) that exhibited no obvious damage or anomalies. Samples ranged from about 6 to 10 weeks (42–70 days) post-fertilization. PE was defined as embryos that were more developed than those at CS23 (i.e., greatest length between 29.2 and 38.6 mm, approximately 8–10 weeks after fertilization) (O’Rahilly and Müller, 2006).

Image acquisition and data analysis

The 3D PCXT image acquisition conditions are described elsewhere (Yoneyama et al., 2011). Briefly, specimens were visualized with a phase-contrast imaging system fitted with a crystal X-ray interferometer (Yoneyama et al., 2004). The system was set up at the vertical wiggler beam line (PF BL14C) of the Photon Factory in Tsukuba, Japan. The white synchrotron radiation emitted from the wiggler was monochromated by a double-crystal monochromator using Si(220), expanded horizontally by an asymmetric crystal, and input into the imaging system. Generated interference patterns were detected by a large-area X-ray imager composed of a 30- μm scintillator, relay lens system, and water-cooled charge-coupled device camera (36×36 mm field of view, 2048×2048 pixels, 18×18 μm each) (Momose, et al., 2001). The X-ray energy was tuned at 17.8 keV, and an exposure time of 3 s was used to obtain one interference pattern. The average intensity was about 300 counts $\text{pixel}^{-1}\text{s}^{-1}$, which allowed fine observations within a reasonable measurement time.

MR images were acquired using a 7T MR system (BioSpec 70/20 USR; Bruker Biospin MRI GmbH; Ettlingen, Germany) with a 35-mm-diameter ^1H quadrature transmit-receive volume coil (T9988; Bruker Biospin MRI GmbH). The 3D T1-weighted images were acquired using a fast, low-angle shot pulse sequence with the following parameters: repetition time, 30 ms; echo time, 4.037–6.177 ms; flip angle, 40° ; field of view, $22.5 \times 15.0 \times 15.0$ – $42.0 \times 28.0 \times 28.0 \mu\text{m}^3$; matrix size, $636 \times 424 \times 424$ – $768 \times 512 \times 512$; and spatial resolution, 35.4 – $54.7 \mu\text{m}^3$.

PCXT was used to acquire 3D images of samples between CS17 and CS21, whereas MRI was used for samples at CS22 and later stages. The method of image acquisition was selected based on sample resolution and volume; that is, PCXT was used to acquire images at a higher resolution than could be obtained by MRI, but could not acquire images of samples with large volumes such that CS21 embryos represented the upper limit in terms of size.

PCXT and MRI data from selected embryos were analyzed precisely as serial 2D and reconstructed 3D images. The structure of the inner ear was reconstructed in all samples using Amira software version 5.4.5 (Visage Imaging; Berlin, Germany). To measure the length of the cochlear duct (CD) and anterior, posterior, and lateral semicircular ducts (SDs) (Fig. 1A), the software module AmiraSkel was used to extract and determine the center line lengths of the CD and anterior, posterior, and lateral SDs. Inner ear length (IEL), maximum length between the endolymphatic sac and CD, the distance between the tip and plane of the basal turn of the CD (Lcdh), and the angle between the cochlear and vestibular parts ($\angle\text{cdv}$) were also measured (Fig. 1B).

Anatomical landmarks and position of the inner ear

The 3D coordinates were initially assigned by examining the voxel position on 3D images using Amira (Fig. 1C, D). Bilateral lens vesicles, which become part of the eyes, were used as external anatomical landmarks. The infundibulum of the diencephalon (later pituitary gland) (Pg) and the cranial region of the first cervical vertebra (C1) were defined as internal anatomical landmarks, while the line connecting the Pg and C1 served as the reference (z-axis) of 3D orthogonal coordinates (Gasser, 2006; Kagurasho et al., 2012). Dorsal and ventral points along the endolymphatic duct (Edd and Edv, respectively) were selected as representative inner ear landmarks. The lines connecting Edd and Edv served as the axis of the inner ear (Ax). The tilt angle between mid-sagittal

plane, z-axis, and Ax was calculated using the 3D coordinates, while $\angle a$ and $\angle b$ were defined as the angles from the cranial view between the Ax and the mid-sagittal plane, and from the lateral view between the Ax and z-axis, respectively. $\angle c$ was defined as the angle between the lateral SD and the z-axis.

Results

Morphology of the inner ear membranous labyrinth

Three dimensional reconstruction revealed the precise morphology of the inner ear membranous labyrinth at each CS (Fig. 2 and Supplemental Videos 1–8). The otic vesicle elongated along the dorso-ventral axis, curving along the lateral side of the rhombencephalon, which differentiated into the end lymphatic appendage and CD at CS17. The primordium of the SDs was visible as a broad triangular elevation in the middle of the otic vesicle at CS17. In two of six organs, no SDs were formed, while all three ducts formed in four of the organs at CS18. SDs were observed in all samples after CS19. The anterior and posterior SDs were visible as prominent circles with a common crus starting from CS18, while the lateral SD appeared as a small, skewed circle lacking a common crus to the anterior and posterior SD (Fig. 3). The anterior SD was the largest and present in one plane, while the lateral SD was twisted in the lateral view (Fig. 3C). The angle between the anterior and posterior SDs appeared wide at initial formation (between CS18 and 21), although they could not be measured owing to their small size and bending.

The CD differentiated and elongated at CS17, and bending in the medial direction between the cochlear and vestibular parts was observed in the latero-caudal view (Fig. 2B). The edge of the angle became more prominent as development proceeded (Table 1 and $\angle c dv$ in Fig. 2B); $\angle c dv$ gradually decreased from 132.5° at CS18 to 112.5° at PE. The spiral course of the CD began from CS18. The CDs had less than a quarter turn at CS19; a quarter- to half-turn was visible at CS20, while at CS21 a half- or full turn was visible. At CS22, there were 1–1.5 turns; at CS23, 1.5–2 turns; and more than two turns were detected at the PE phase in all samples. CDs remained in nearly the same plane until CS23, at which time their heights could be discerned (blue arrow in Fig. 2B [PE]). $Lcdh$ was 0.17 mm at CS22 and CS23, and increased to 0.42 mm at PE (Table 1).

The endolymphatic duct elongated and the endolymphatic sac swelled starting from CS18, assuming a flat and spoon-like shape at CS22. The appearance of the endolymphatic sac varied across samples. The saccule and ductus reuniens were visible in all samples after CS22 (Fig. 2B). In the membranous labyrinth, the posterior canal was shifted downwards over the lateral canal (red and green arrows in Fig. 3), while the cochlea was displaced forwards and upwards at the PE phase (black arrow in Fig. 3), as

previously described (Sercer and Krmpotic, 1958). The three SDs were almost vertical with respect to each other at this phase.

Length of CD and SDs

The length of the SDs increased linearly over the course of development (Fig. 4). At every stage, the length of SDs was greatest in the anterior ducts, followed by the posterior and then lateral ducts. The length ratio of the anterior to lateral SDs was between 1.55 and 1.31, while ratios of 1.15 and 1.36 were determined between the posterior and lateral SDs (Table 1). The length ratios were nearly constant during the observation period. The length of the CD increased exponentially and exceeded the length of anterior SDs at CS23.

Position of the inner ear membranous labyrinth with respect to the embryonic brain

The bilateral inner ear membranous labyrinth was located lateral to the ventral side of the rhombencephalon and caudal to the pontine flexure next to the auditory ganglia. The inner ear persisted during the observation period, as demonstrated by the 3D coordinates, with Pg and C1 serving as points of reference (Fig. 5, Table 2). The Edvs located 0.63 and 1.74 mm dorsal to the Pg-C1 lines (Lvz in Figure 1C) as well as the Lvc to Lpc ratio remained almost constant (i.e., between 0.42 and 0.47) after CS 18 (Table 2). The axis of the endolymphatic ducts (Ax) was tilted after CS18 (Fig. 5); $\angle a$ was between 39.9° and 43.7° , whereas $\angle b$ was between 48.0° and 62.9° after CS18. The tilt angle between the plane of the lateral SD and z-axis ($\angle c$) was at 8.0° – 14.6° between CS19 and PE, indicating that the plane was never oriented horizontally during the observation period (Fig. 5, Table 2).

Although precise morphometry was not applied in the present study owing to the small size and complexity of the inner ear at the developmental stages examined, the following features are worth noting (Fig. 5 and Supplementary Video 9). CDs were located on the latero-ventral side of the pontine, and the vector normal to the CD plane was mostly oriented in the direction of the auditory ganglion (blue arrows in Fig. 2B). The orientation of Ax was similar to that of the common crus (Fig. 2BC).

Discussion

The differentiation of the inner ear membranous labyrinth from CS17 to PE was investigated by 3D analysis. The time course of SD formation at each CS was consistent with those reported in previous studies (O’Rahilly, 1983; Arnold and Lang, 2001; Yasuda et al., 2007). The major findings were as follows. The three SDs in order of decreasing size were anterior, posterior, and lateral; the order was established starting from CS18. The morphological features and developmental time course of the lateral SD differed from those of anterior and posterior structures, developing more slowly at CS17 and assuming a small, skewed, and twisted shape. The posterior canal extended downwards over the lateral canal, which is a prominent feature in humans (Sercer and Krmpotic, 1958) that became increasingly obvious during the observation period. Finally, the angle between the anterior and posterior SDs was wide at initial formation (between CS18 and CS21), although it could not be precisely measured owing to the small size and torsion of these structures. The three SDs were almost vertical with respect to each other at the PE phase. The relationship among the three SDs in adults is controversial, with several studies reporting a wide angle (104° – 111°) between anterior and posterior SDs (Spoor et al., 1998; El Khoury et al., 2014) and others describing the three SDs as being almost parallel to each other (Hashimoto et al., 2005; della Santina et al., 2005), as observed in the present study.

The spiral turn of the CD was unique and gave this structure a distinct morphology. Previous studies have described the relationship between developmental stage and the turn of the CD. The coiling of the CD was first detected at CS18, as described in earlier reports (Streeter, 1951; Gasser, 1975; O’Rahilly and Müller, 1987; Yasuda et al., 2007; Arnold and Lang, 2001). However, the time taken for completion of the spiral turns is unclear. Previous studies based on CS found that the CD completes 2.5 turns (a definitive number) at CS23 (Streeter, 1951; Gasser, 1975; O’Rahilly and Müller, 1987); however, another report found that 30-mm embryos had between 1 and 1.5 turns while 40- to 50-mm embryos had 2.5 turns (Altman, 1950). We observed that the CD was discoid with about 1.5–2 turns in almost the same plane at CS23, and was conical with > 2 turns at the PE phase. The 3D data indicated that the CD was still in the process of coiling at CS23.

The spatial relationship between the cochlear and vestibular parts of the inner ear was revealed by the 3D analysis. There was bending in the medial direction between

the two parts in the latero-caudal view, while the cochlea showed forward (in the cranial direction) and upward displacement at the PE phase during the observation period. These changes are prominent features of the developing human membranous labyrinth (Sercer and Krmpotic, 1958). A morphometric and morphological analysis of bone labyrinth was recently carried out in embryos at 9.4 to 29.2 weeks of gestation (Jeffery and Spoor, 2004); that is, immediately following the embryonic stages examined in the present study. The SDs were comparable in size to those measured in the previous study, although we measured the centerline length of the three SDs of the membranous labyrinth, whereas the other study measured the semicircular canal radius of the bone labyrinth, which was reconstructed in the fetal periods and was similar to our reconstruction at the PE phase. However, their detailed morphometric analysis indicated that the early fetal bone labyrinth differed significantly from the structure in adults. In our samples, the membranous labyrinth was too small to measure; a higher resolution imaging method is necessary for a detailed morphometric analysis and comparisons between fetal and adult structures.

We estimated the movement of the external ear using Pg and C1 (z-line) as reference points, and found that the external ear did not undergo migration and that any movement—which was mostly in the lateral and not cranial direction—can be explained as differential growth (Gasser, 2006). We have previously described the movement of the inner ear (vestibule), which remains next to the pontine (Kagurasho et al., 2012). The distance between the inner and outer ears was nearly constant throughout development, although their relative positions changed. Our detailed study of the inner ear by high-resolution PCXT and MRI revealed limited movement of this structure during the embryonic period. A recent report indicated that the close proximity of the inner ear and hindbrain and mesenchyme is necessary for normal development (Liang et al., 2010; Nakajima, 2015).

It is worth noting that the lateral SD was almost parallel (8.0° – 14.6°) to the z-(Pg-C1) axis during the observation period, consistent with previous observations (Blechschiidt, 1961; Streeter, 1906; O’Rahilly and Müller, 2006). The lateral SD is also referred to as the horizontal SD, and is typically depicted in the horizontal orientation in textbook illustrations (Drake et al., 2005) and 3D models of the lateral cranium. The actual position of the lateral semicircular canal was about 20° – 25° above the Z-REID plane (della Santina et al., 2005; El Khoury et al., 2014) and/or 30° above

the horizontal plane (Parnes et al., 2003). On the other hand, the line connecting the references (Pg and C1) was orthogonal to the horizontal plane in adults, suggesting that the orientation of the inner ear changes drastically after embryogenesis.

A recent study showed that the lateral bone could be reconstructed in three dimensions except around the bone labyrinth (Gussen, 1968; Sørensen et al., 2007). It has been suggested that the fetal labyrinth shows little or no change in shape after attaining the adult size and becoming embedded in the ossified otic capsule; however, the orientation may change, given that the development and differentiation of the brain influence construction on the basal cranium and pyramid (petrous bone) (Jeffery and Spoor, 2002). In addition, environmental factors such as the erect posture adopted after birth—which causes changes to the base of the skull and consequently, produces forces that act on the labyrinthine capsule and alter its position as well as its shape—must be taken into account (Sercer and Krmpotic, 1958; Spoor et al., 2003).

The present 3D analysis describes the time course of differentiation of the inner ear membranous labyrinth from CS17 to the PE phase, providing novel insight into how the orientation of the inner ear changes with respect to the body during development and growth, from embryonic stages to adulthood.

Acknowledgments

This work was partly supported by the Innovative Techno-Hub for Integrated Medical Bio-imaging of the Project for Developing Innovation Systems, from the Ministry of Education, Culture, Sports, Science and Technology of Japan. This work was carried out under the approval of the Photon Factory Program Advisory Committee (proposal nos. 2013G514, 2012G138, and 2014G018). The authors thank Dr. Kazuyuki Hyodo (Associate Professor of the SR Science Division II of the Institute of Materials Structure Science) for providing access to the phase-contrast X-ray, and Dr. Kohei Shiota (President of Shiga University of Medical Science) for providing the invaluable MR data.

References

- Altmann F. 1950. Normal development of the ear and its mechanics. *AMA Arch Otolaryngol* 52:725–766.
- Arnold WH, Lang T. 2001. Development of the membranous labyrinth of human embryos and fetuses using computer aided 3D-reconstruction. *Ann Anat* 183:61–66.
- Bast TH, Anson BJ, Gardner WD. 1947. The developmental course of the human auditory vesicle. *Anat Rec* 99:55–74.
- Blechsmidt E. 1961. Human embryos In: *The stages of human development before birth: an introduction to human embryology*. Philadelphia: Saunders. p 39–232.
- Della Santina CC, Potyagaylo V, Migliaccio AA, Minor LB, Carey JP. 2005. Orientation of human semicircular canals measured by three-dimensional multiplanar CT reconstruction. *J Assoc Res Otolaryngol* 6:191–206.
- Drake RL, Vogl AW, Mitchell AWM. 2005. *Gray's Anatomy for students*. Philadelphia: Elsevier/Churchill Livingstone.
- El Khoury M, Braga J, Dumoncel J, Nancy J, Esclassan R, Vaysse F. 2014. The human semicircular canals orientation is more similar to the bonobos than to the chimpanzees. *PLoS ONE* 9:e93824.
- Gasser RF. 2006. Evidence that some events of mammalian embryogenesis can result from differential growth, making migration unnecessary. *Anat Rec B New Anat* 289:53–63.
- Gasser RF. 1975. The eighth week of life, left embryonic period. In: *Atlas of Human Embryos*, 1st ed. Hagerstown: Harper and Row. p. 241–259.
- Gitton Y, Heude E, Vieux-Rochas M, Benouaiche L, Fontaine A, Sato T, Kurihara Y, Kurihara H, Couly G, Levi G. 2010. Evolving maps in craniofacial development. *Semin Cell Dev Biol* 21:301–308.
- Gunz P, Ramsier M, Kuhrig M, Hublin JJ, Spoor F. 2012. The mammalian bony labyrinth reconsidered, introducing a comprehensive geometric morphometric approach. *J Anat* 220:529–543.
- Gussen R. 1968. Articular and internal remodeling in the human otic capsule. *Am J Anat* 122:397–417.
- Hashimoto S, Naganuma H, Tokumasu K, Itoh A, Okamoto M. 2005. Three-dimensional reconstruction of the human semicircular canals and

- measurement of each membranous canal plane defined by Reid's stereotactic coordinates. *Ann Otol Rhinol Laryngol* 114:934–938.
- Jeffery N, Spoor F. 2002. Brain size and the human cranial base: a prenatal perspective. *Am J Phys Anthropol* 118:324–340.
- Jeffery N, Spoor F. 2004. Prenatal growth and development of the modern human labyrinth. *J Anat* 204:71–92.
- Kagurasho M, Yamada S, Uwabe C, Kose K, Takakuwa T. 2012. Movement of the external ear in human embryo. *Head Face Med* 8:2.
- Liang JK, Bok J, Wu DK. 2010. Distinct contributions from the hindbrain and mesenchyme to inner ear morphogenesis. *Dev Biol* 337:324–334.
- Momose A, Takeda T, Yoneyama A, Koyama I, Itai Y. 2001. Wide-area phase-contrast x-ray imaging using large x-ray interferometers. *Nucl Instrum Methods A* 467:917–920.
- Nakajima Y. 2015. Signaling regulating inner ear development: Cell fate determination, patterning, morphogenesis, and defects. *Congenit Anom (Kyoto)* 55:17–25.
- Nishimura H, Takano K, Tanimura T, Yasuda M. 1968. Normal and abnormal development of human embryos: first report of the analysis of 1,213 intact embryos. *Teratology* 1:281–290.
- O'Rahilly R. 1983. The timing and sequence of events in the development of the human eye and ear during the embryonic period proper. *Anat Embryol (Berl)* 168:87–99.
- O'Rahilly R, Müller F. 1987. Stage 19. In: *Developmental stages in human embryos: including a revision of Streeter's Horizons and a survey of the Carnegie Collection*. Washington, D.C.: Carnegie Institution of Washington. p. 239–251.
- O'Rahilly R, Müller F. 2006. Stage 20, Stage 21. In: *The embryonic human brain: an atlas of developmental stages*, 3rd ed. Hoboken: Wiley-Liss. p. 169–204.
- Parnes LS, Agrawal SK, Atlas J. 2003. Diagnosis and management of benign paroxysmal positional vertigo (BPPV). *CMAJ* 169:681–693.
- Richard C, Laroche N, Malaval L, Dumollard JM, Martin C, Pech M, Vico L, Prades JM. 2010. New insight into the bony labyrinth: a microcomputed tomography study. *Auris Nasus Larynx* 37:155–161.
- Sercer A, Krampotic J. 1958. Further contribution to the development of the labyrinthine capsule. *J Laryngol Otol* 72:688–698.

- Shiota K. 1991. Development and intrauterine fate of normal and abnormal human conceptuses. *Congenit Anom (Kyoto)* 31:67–80.
- Spoor F, Hublin JJ, Braun M, Zonneveld F. 2003. The bony labyrinth of Neanderthals. *J Hum Evol* 44:141–165.
- Spoor F, Zonneveld F. 1995. Morphometry of the primate bony labyrinth: a new method based on high-resolution computed tomography. *J Anat* 186:271–286.
- Sørensen MS, Frisch T, Bretlau P. 2007. Dynamic bone studies of the labyrinthine capsule in relation to otosclerosis. *Adv Otorhinolaryngol* 65:53–58.
- Streeter GL. 1906. On the development of the membranous labyrinth and the acoustic and facial nerves in the human embryo. *Am J Anat* 6:139–165
- Streeter GL. 1917. The factors involved in the excavation of the cavities in the cartilaginous capsule of the ear in the human embryo. *Am J Anat* 22:1–25.
- Streeter GL. 1918. The histogenesis and growth of the otic capsule and its contained periotic tissue-spaces in the human embryo. *Contrib Embryol Carneg Instn* 7:5–54.
- Streeter, GL. 1951. Developmental horizons in human embryos. Description of age groups XTX, XX, XXI, XXII, and XXIII, being the fifth issue of a survey of the Carnegie Collection (prepared for publication by C. H. Heuser and G. W. Corner). *Carnegie Instn. Wash. Publ.* 592, *Contrib. Embryol.*, 34, 165–196.
- Yamada S, Uwabe C, Fujii S, Shiota K. 2004. Phenotypic variability in human embryonic holoprosencephaly in the Kyoto Collection. *Birth Defects Res A Clin Mol Teratol* 70:495–508.
- Yasuda M, Yamada S, Uwabe C, Shiota K, Yasuda Y. 2007. Three-dimensional analysis of inner ear development in human embryos. *Anat Sci Int* 82:156–163.
- Yoneyama A, Yamada S, Takeda T. 2011. Fine biomedical imaging using X-ray phase-sensitive technique. In: Gargiulo G, editor. *Advanced Biomedical Engineering*, Vol. 1. Rijeka: InTech. pp. 107–128.
- Yoneyama A, Takeda T, Tsuchiya Y, Wu J, Lwin TT, Koizumi A, Hyodo K, Itai Y. 2004. A phase-contrast X-ray imaging system-with a 60 x 30 mm field of view based on a skew-symmetric two-crystal X-ray interferometer. *Nucl Instrum Methods Phys Res A* 523:217–222.

Figure legends

Figure 1. Definition of the reference axis, anatomical landmarks, and morphometry in the present study.

A: Latero-cranial view illustrating the morphometry of the inner ear.

The broken line indicates the center line of semicircular and cochlear ducts used for measurements. A, anterior (blue); CD, cochlear duct (black); L, lateral (green); P, posterior (red).

B: Caudo-lateral view showing the basal turn of the CD in a single line.

IEL; inner ear length representing the maximum length between the endolymphatic sac and CD; Lcdh, distance between the tip and plane of the basal turn of the CD; $\angle c dv$, angle between cochlear and vestibular parts.

C, D: Cranial (C) and lateral (D) views of anatomical landmarks used to measure the position of the inner ear.

Ax, axis of the endometrial duct; C1, first cervical vertebra; Edd and Edv, dorsal and ventral points, respectively, along the endolymphatic duct; Ev, eye vesicle; Pg, pituitary gland; $\angle a$, tilt angle between the axis of endolymphatic duct and mid-sagittal plane; $\angle b$, tilt angle between the axis of endolymphatic duct and z-axis; $\angle c$; angle between the lateral semicircular duct and z-axis, Lvz; distance between Edv and z-axis, Lpc; length between Pg and C1, Lvc; length between Edv and C1 along the z-axis.

Figure 2. Morphology of the left inner ear from CS17 to the PE phase (greatest length, 38.6 mm).

A: Representative images of the MRI and PCXT for the reconstruction of inner ear.

Red line indicates the plane corresponding to the transverse sections a, b, and c in the 3D reconstruction. Di; diencephalon, E; external auditory meatus, M; middle ear, Oc; otic capsule, p; pinna, Ro; rombencephalon, v; trigeminal ganglia, viii; auditory and facial ganglion.

B: Left caudo-lateral view. In the end lymphatic appendage, the CD (purple) was observed laterally and the SDs (yellow) were visible.

C: Left latero-cranial view. The anterior SD, turns in the CD, endolymphatic sac (Es), and saccule (S) were visible. A, anterior; CD, cochlear duct; L, lateral; P, posterior; PE,

postembryonic; U, utricle; ○; common crus. Scale bar = 1 mm.

Figure 3. Morphology of the left inner ear illustrating the spatial relationship between the three SDs at the PE phase (greatest length, 38.6 mm).

The three SDs were vertical and parallel to each other; the anterior SD was circular, while the lateral SD was twisted. A, anterior; CD, cochlear duct; ○, common crus; Dr, ductus reuniens; Es, endolymphatic sac; L, lateral; P, posterior; S, saccule. Scale bar = 1 mm.

Figure 4. Length of the inner ear, CD, and three SDs from CS18 to the PE phase.

A, anterior; C, cochlear duct; IEL, inner ear length; L, lateral; P, posterior.

Figure 5. Relative positions of the embryonic brain and inner ear.

3D reconstructions of the inner ear and brain (upper), and illustrations from reconstructions based on PCXT images at CS18 and MR images at PE (lower). Pg, pituitary gland; C1, cranial part of the first vertebra. The caudal cranial (z-) axis is indicated by a broken line.

Figure 6. Position of the inner ear from CS 18 to PE phase.

∠a; angle from the cranial view between the axis of the endometrial duct (Ax) and the mid-sagittal plane, ∠b; angle from the lateral view between the Ax and z-axis, ∠c; angle between the lateral SD and z-axis. The measured angle is indicated in Figure 1C and D.

Supplemental Videos 1–8.

Morphology of the inner ear from CS17 to the PE phase (greatest length, 38.6 mm).

Supplemental Videos 9 and 10.

Relative positions of the embryonic brain and inner ear from CS 18 to the PE phase (greatest length, 43.5 mm).

Table 1. Length measurements of inner ear structures

Carnegie Stage	Inner ear		Cochlear ducts						Semicircular ducts (length in mm)						Length ratio of SDs			
	length		Length		Lcdh		\angle cdv		ASD		PSD		LSD		ASD/LSD		PSD/LSD	
	Mean	s.d.	Mean	s.d.	Mean	s.d.	Mean	s.d.	Mean	s.d.	Mean	s.d.	Mean	s.d.	Mean	s.d.	Mean	s.d.
18	2.13	0.13	1.25	0.14	ND		132.5	2.5	2.33	0.07	1.98	0.23	1.65	0.13	1.43	0.15	1.21	0.19
19	2.25	0.23	1.43	0.23	ND		131.3	5.5	2.71	0.35	2.36	0.23	2.09	0.32	1.31	0.12	1.15	0.12
20	2.74	0.08	2.34	0.17	ND		125.8	4.6	3.82	0.27	2.96	0.10	2.56	0.21	1.50	0.12	1.16	0.12
21	3.00	0.12	2.70	0.56	ND		128.5	4.0	4.12	0.25	3.40	0.26	2.67	0.15	1.55	0.13	1.28	0.15
22	3.39	0.25	3.87	0.27	0.17	0.04	113.7	5.4	4.29	0.13	3.78	0.57	2.79	0.12	1.54	0.07	1.36	0.25
23	4.21	0.31	6.33	0.33	0.17	0.02	121.7	4.7	5.27	0.31	4.45	0.12	3.45	0.16	1.53	0.08	1.29	0.07
PE	5.53	0.72	11.18	2.69	0.42	0.11	112.5	10.4	6.80	1.20	6.06	1.49	5.22	1.07	1.32	0.16	1.15	0.07

SD, semicircular duct; ASD, anterior SD; PSD, posterior SD; LSD, lateral SD; s.d., standard deviation; PE, post-embryonic phase;

ND, not determined; Lcdh, distance between the tip and plane of basal turn of cochlear duct; \angle cdv; angle between cochlear and vestibular parts.

Table 2. Position of the inner ear membranous labyrinth with respect to the embryonic brain

Carnegie Stage	No. of organs	Greatest length (mm)	Length (mm)						Ratio		Tilt angle (degrees)					
			Lvz		Lvc		Lpc		Lvc/Lpc		∠a		∠b		∠c	
			Mean	s.d.	Mean	s.d.	Mean	s.d.	Mean	s.d.	Mean	s.d.	Mean	s.d.	Mean	s.d.
17	10	8.8–11.5	1.16	0.08	1.60	0.15	2.81	0.09	0.57	0.04	84.0	21.0	105.2	17.7	ND	
18	6	10.5–12.7	0.88	0.08	1.27	0.19	2.84	0.35	0.45	0.04	41.8	5.7	60.8	22.5	ND	
19	8	12.1–12.9	0.80	0.06	1.41	0.28	2.97	0.32	0.47	0.06	39.9	5.3	62.9	17.0	13.0	2.5
20	6	16.0–17.6	0.63	0.23	1.38	0.21	3.13	0.21	0.44	0.04	41.2	4.9	56.8	15.2	12.4	3.2
21	6	17.6–18.9	0.68	0.09	1.30	0.10	3.14	0.08	0.42	0.03	43.0	3.7	48.0	12.5	8.0	2.2
22	6	20.1–22.6	0.68	0.17	1.54	0.31	2.84	0.18	0.42	0.07	43.5	1.5	58.4	5.9	8.8	2.0
23	6	24.4–30.6	0.89	0.00	2.06	0.19	2.81	0.10	0.44	0.03	43.7	2.3	52.5	12.6	14.6	3.6
PE	6	29.2–38.6	1.64	0.30	2.84	0.57	2.81	1.10	0.46	0.03	42.3	1.5	57.2	5.4	11.6	3.4

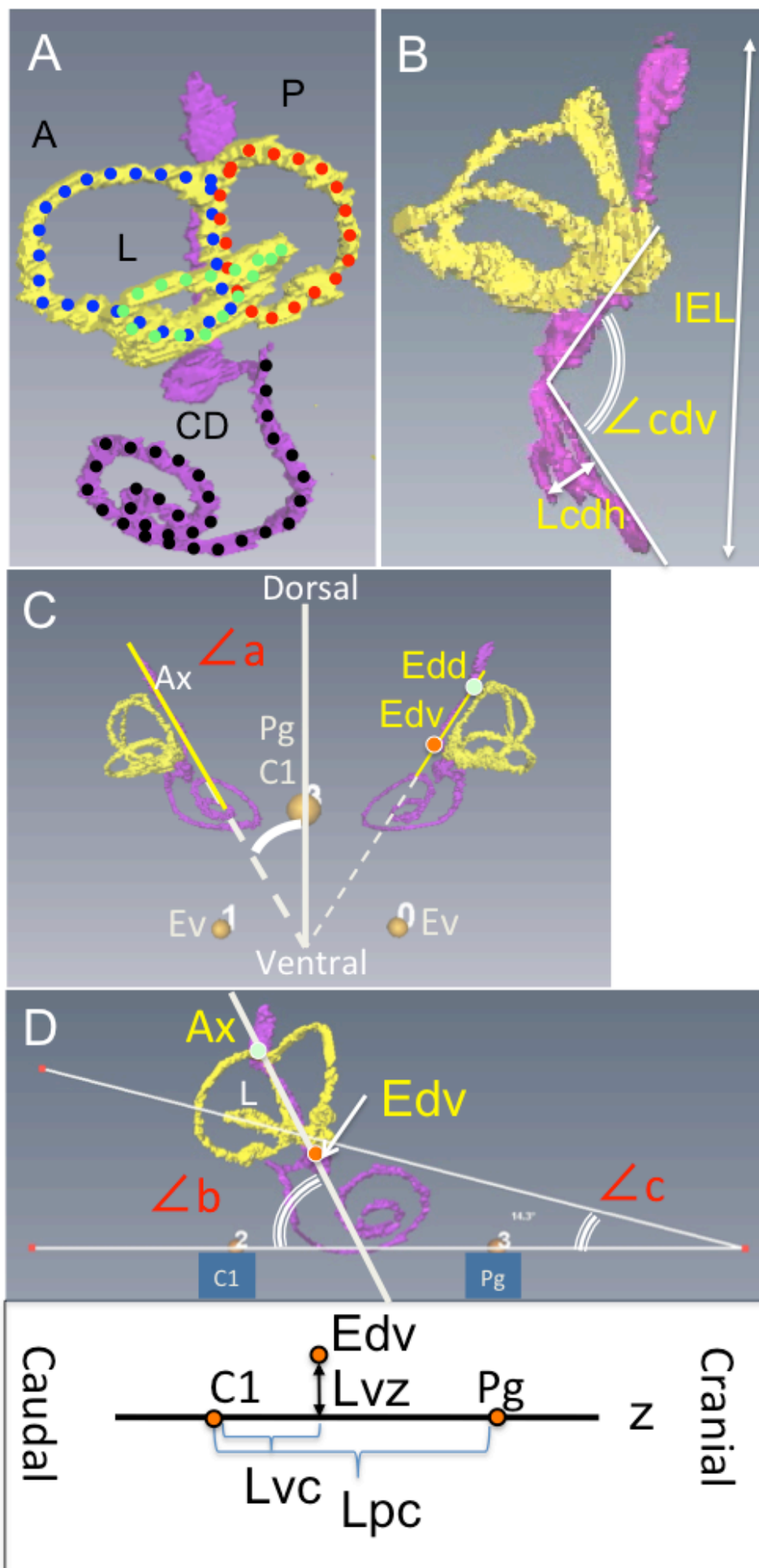
PE, post embryonic stage; ND, not determined; s.d., standard deviation.

∠a, angle from the cranial view between the axis of the endometrial duct (Ax) and the mid-sagittal plane;

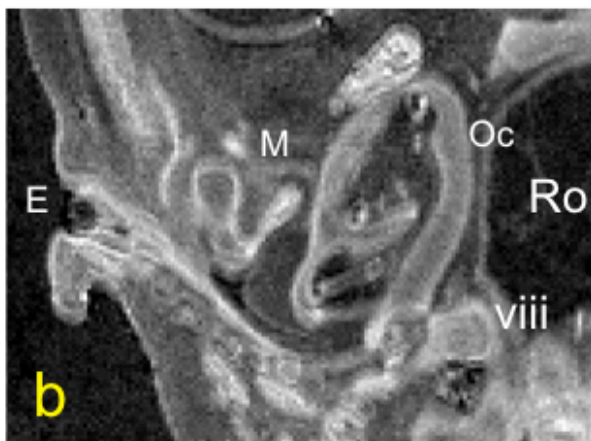
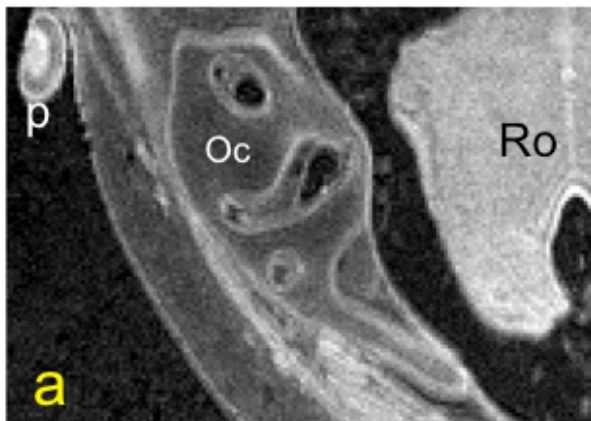
∠b, angle from the lateral view between the Ax and z-axis; ∠c, angle between the lateral semicircular duct and z-axis.

Lvz, distance between a ventral point along the endolymphatic duct (Edv) and z-axis;

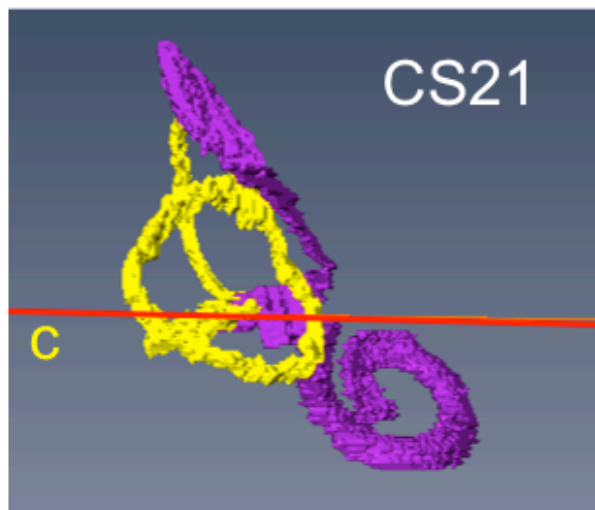
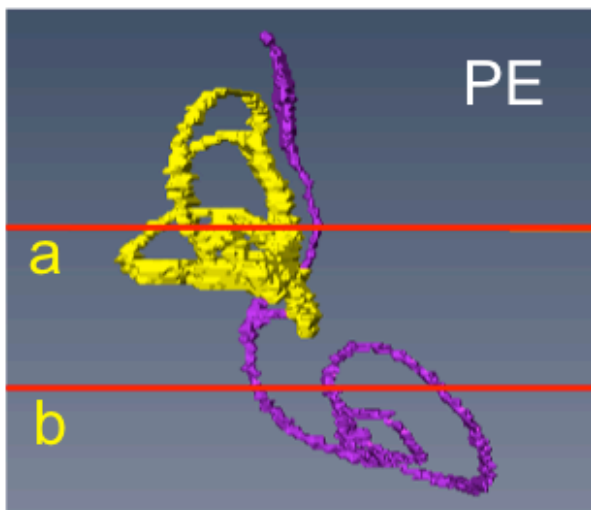
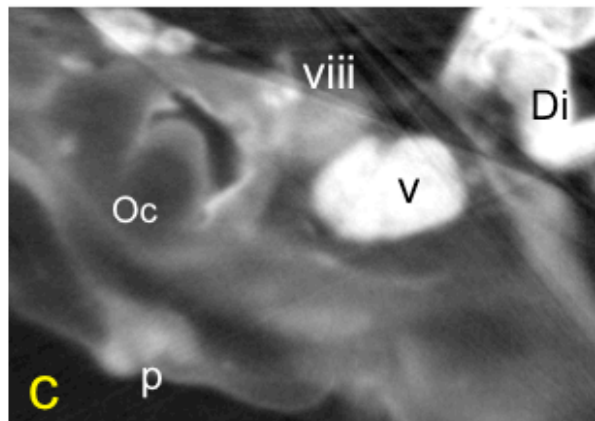
Lpc, length between the pituitary gland and cranial region of the first cervical vertebra (C1); Lvc, length between Edv and C1 along the z-axis.



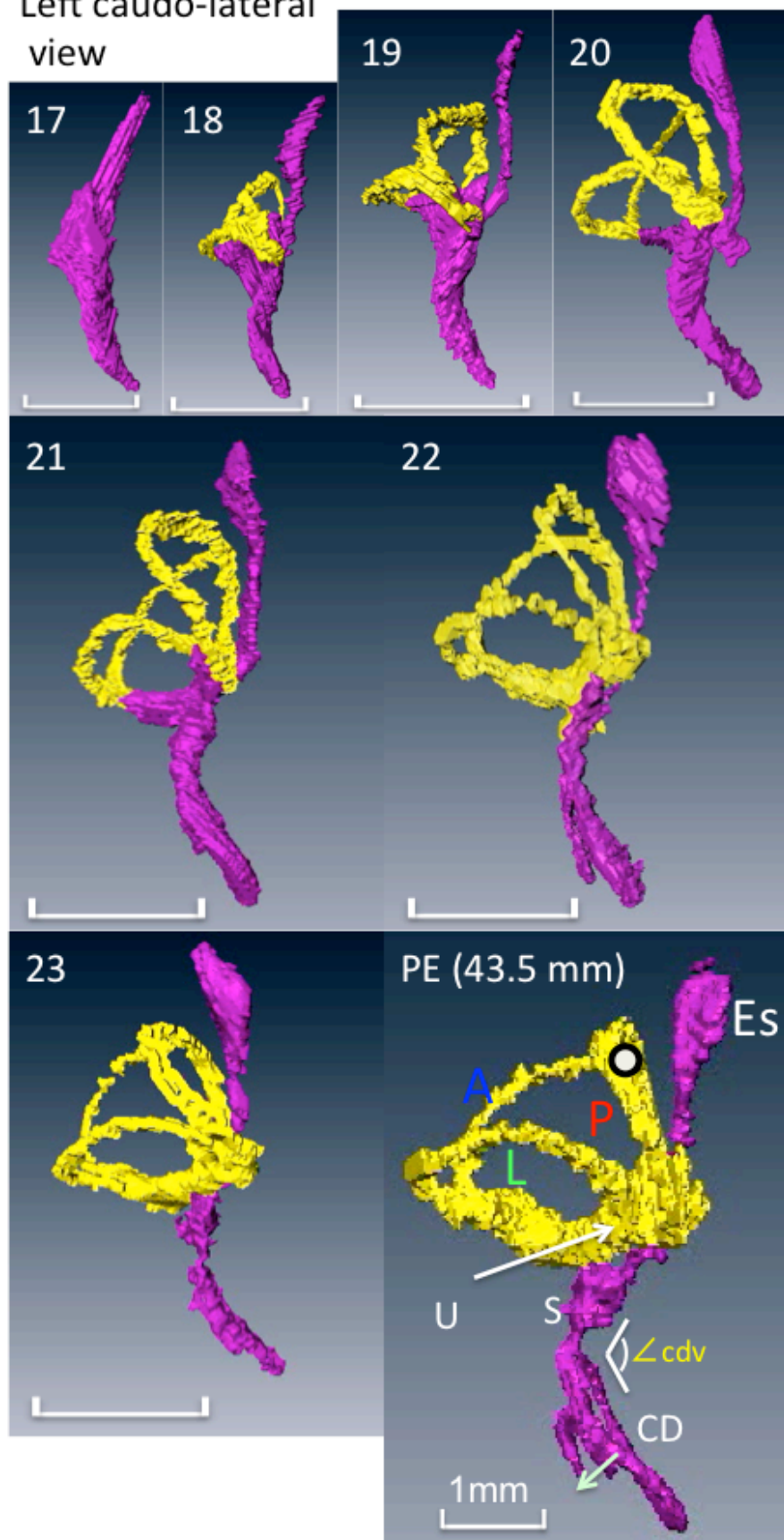
MRI



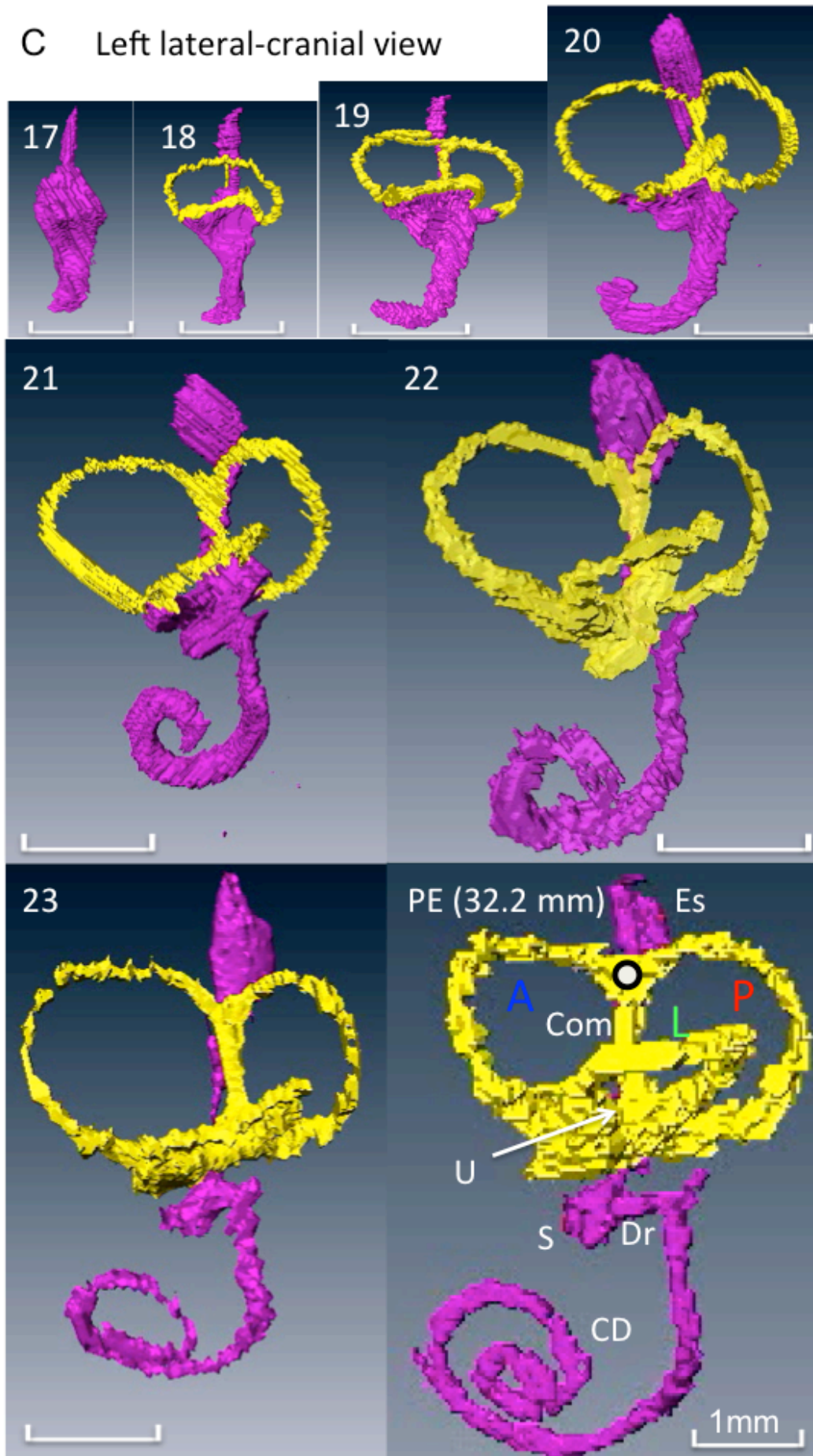
PCXT

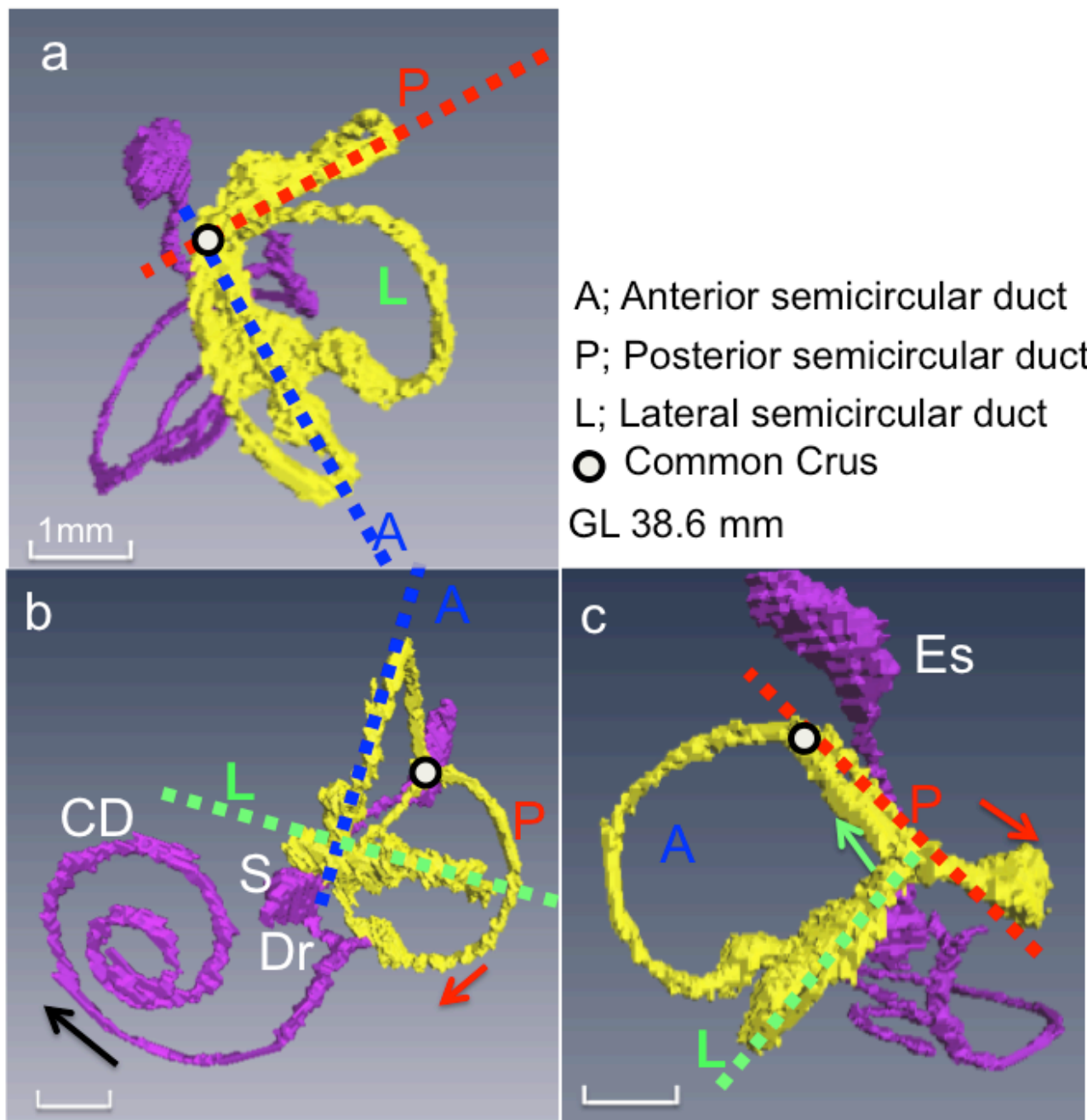


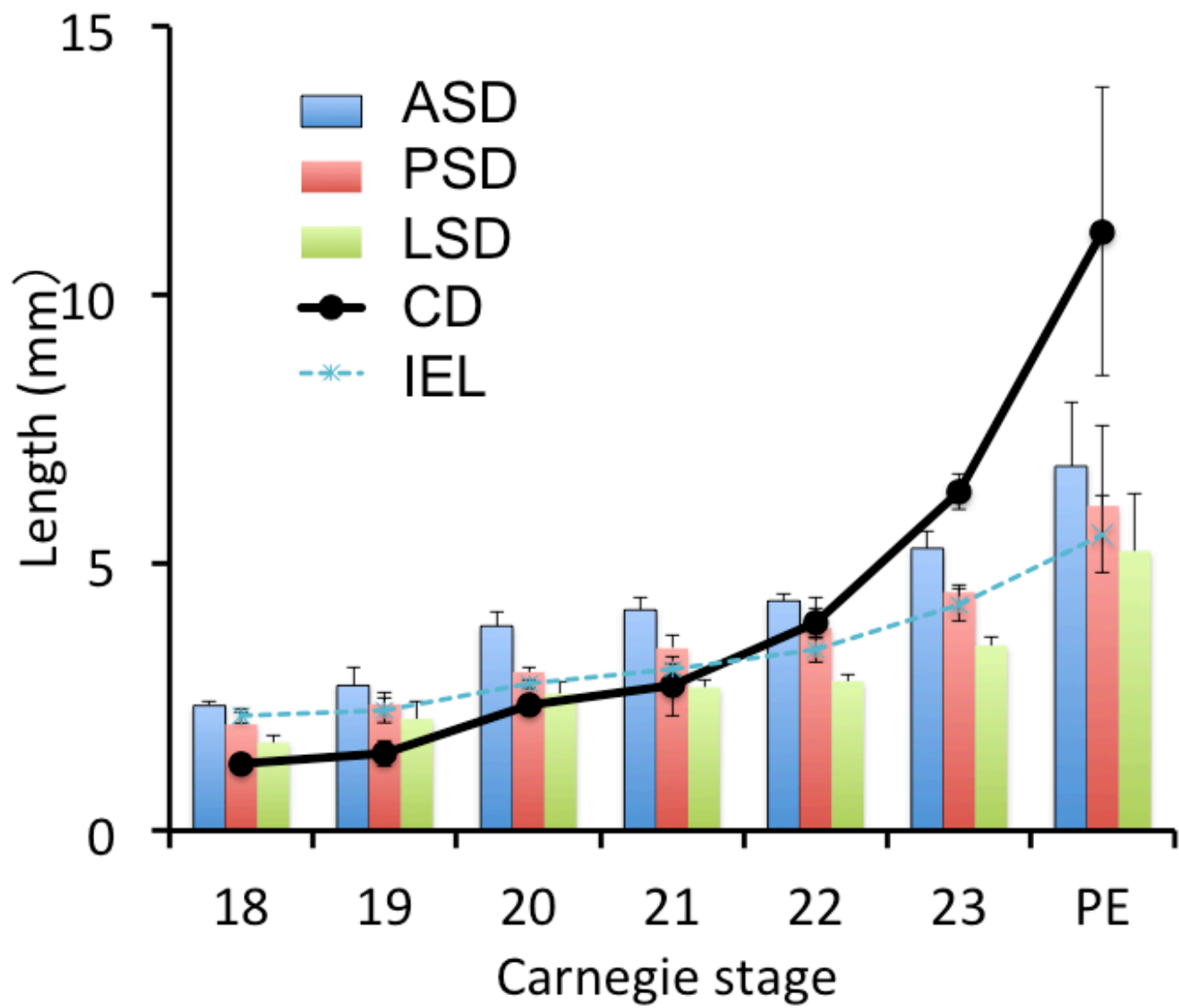
B Left caudo-lateral
view

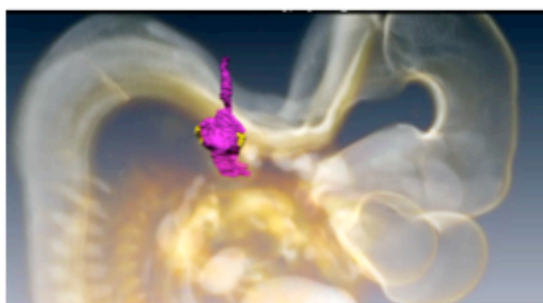


C Left lateral-cranial view

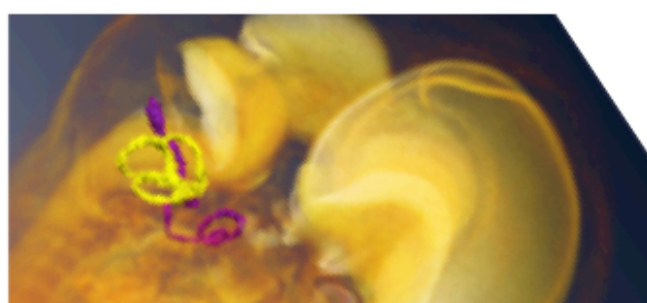
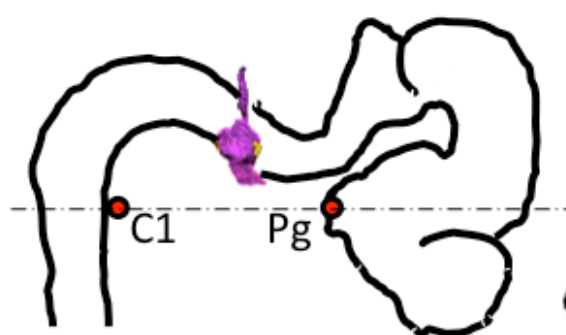








18



PE

